eJSE International

Electronic Journal of Structural Engineering (8) 2008

Experimental and theoretical dynamic system identification of damaged RC beams

F. Daneshjoo & A. Gharighoran
Civil Engineering Department,Faculty of Engineering,Tarbiat Modares University, Tehran, Iran
Email: danesh_f@modares.ac.ir

ABSTRACT: Dynamic system identification of RC beams i.e. natural frequencies, damping ratios and mode shapes is of high importance due to their special role in most civil engineering structures. In this paper, the effects of damage on dynamic characteristics of reinforced concrete beams are investigated experimentally. The possibility of obtaining load displacement curves through dynamic testing for in situ reinforced concrete beams is evaluated and the proposed methods are verified. Damage is considered as reduction in the flexural stiffness with increasing degree of cracking. A vibrating motor with aluminum flywheels to which masses could be attached at varying eccentricities are used for producing the dynamic cyclic loads. The variation in natural frequency, amplitude of vibration, damping and bending stiffness with increasing eccentric mass and for increasing degree of cracking are evaluated through steady state vibration at resonance with gradual increase of concentrated load at mid span. The changes in the secant stiffness with increasing degree of cracking and for increasing and decreasing concentrated static loads are obtained. Damping values are calculated from free vibration decay function using logarithmic decrement method. The results indicate that the damping ratio in the vicinity of the cracked region is not merely viscous, but rather is a combination of viscous and frictional damping. The contribution of the frictional damping will increase by increasing degree of cracking.

*Keywords***:** Dynamic system identification; Damage assessment; Damping; Concrete beam.

1 INTRODUCTION

Identification of dynamic characteristics of any structural system is known as dynamic system identification. Damage is detected by comparing the identified dynamical indices of the damaged and undamaged structures. Due to the special role of the beams in most of the civil engineering structures, dynamic system identification of beams, especially during service time, is of high importance. For example, in case of failure, the beams as an important element of the bridges may cause overall instability of the bridge structure. In this regard, various studies have been conducted. Monitoring of bridges and building based on vibration measurements is widely addressed in literatures, e.g., in Doebling an extensive overview is given [1]. Turner and Pretlove performed a numerical vibration analysis on a simple beam representation of a bridge subjected to random traffic loading [2]. The authors stated that the measured response of a bridge to traffic appears to provide a method of determining resonant frequency. The motivation for the work was the development of a structural condition monitoring system that did not require a measured excitation force. Spyrakos *et al* performed a series of experiments on a set of beams [3]. Each beam was given different damage scenarios (type, location and degree), and low-level free vibration tests were performed. They found a definite correlation between the level of damage and the dynamic characteristics of the structure. Ren and Roeck experimentally developed a methodology of structural damage identification through changes in the dynamic characteristics [4,5]. They used concrete beams stiffness for damage assessment and the proposed methodology relied on the fact that damage leads to changes in the dynamic properties of the structure such as natural frequencies and mode shapes.

The use of damping factor for damage assessment is still in an experimental phases. In the structural engineering, the energy dissipation in real structures is far more complicated, especially when appear damage, and is affected by many parameters. Daneshjoo and Karimi investigated the damping of uncracked and cracked reinforced concrete (RC) beams [6]. They found that damping increases with the development of cracks and that the damping is not viscous in cracked beams. Ndambi studied the damping

mechanism and the use of damping as indicator in structural health monitoring (SHM) to assess damage in partially RC concrete beams [7]. Attempts are also made to use damping ratios as a measure of damage but often they were unsuccessful. Modena *et al*, presented two localization techniques based on damping measurement [8]. The first was based on the vibration of energetically equivalent modal damping ratio and the second was based on distinguishing the contribution of viscous and friction components on damping. Casas *et al*, performed tests on partially cracked concrete beams [9]. The results indicated no clear relation between crack growth and increase of damping. Tests before and after structural repairs to a RC bridge were conducted by Williams and salawu and no clear trend in damping values could be detected [10].

Damage assessment of bridges and other civil engineering structures and structural elements have been performed by many researchers such as Kato , Aktan, Farrar, Peeters, Teughels, Maeck, Mirdamadi, Bakhtiar-Nejad and Boltan and research on these subjects is still of importance and is continued [11-19].

In this paper, the effects of damage on dynamic characteristics of RC beams are investigated experimentally. For this purpose, the dynamic behavior of one simply supported beam with a concentrated load at mid span is studied. A vibrating motor with aluminum flywheels to which masses could be attached at varying eccentricities are used for producing the dynamic cyclic loads. The possibility of obtaining load displacement curves through dynamic testing for in situ RC beam is evaluated and the statically and dynamically obtained load displacements curves are compared. The variation in natural frequency, amplitude of vibration, damping and bending stiffness with increasing eccentric mass and for increasing degree of cracking are evaluated through impulse testing and steady state vibration at resonance with gradual increase of concentrated load at mid span. The damping ratios are calculated by three different methods and equivalent damping mechanism is discussed. The approximate dynamic response of the beam is obtained by considering them as single degree of freedom damped mass spring systems and the equivalent mass, stiffness and damping of the mass spring system are determined.

2 THEORIES

The approximate dynamic response of the simply supported reinforced concrete beam which supports a concentrated load Q at mid span in addition to its weight W, may be obtained by considering them as equivalent single degree of freedom system as shown in Fig. 1. The expressions for equivalent or generalized mass M_e, stiffness K_e and damping coefficient C_e of the equivalent mass spring systems is given by Equations 1, 2 and 3 respectively. To obtain an expression for the equivalent mass, the kinetic energy of the mass spring system is equated to that of the reinforced concrete beam. The expression for the equivalent elastic spring system is found by equating the strain energy stored in the spring to that stored in the RC beam. The expression for the equivalent damping is found by equating the virtual work of the damping force in the mass spring system to the virtual work done by the damping force in the beam.

$$M_e = Q + 2\int_0^{l/2} W[\phi(x)]^2\,dx \tag{1}$$

$$K_e = 2\int_0^{l/2} EI[\phi''(x)]^2\,dx \tag{2}$$

$$C_e = 2\int_0^{l/2} C[\phi(x)]^2\,dx \tag{3}$$

where $\phi(x)$, l and C are the first vibration mode shape, length and damping coefficient of the RC beam respectively.

The dynamic response of the equivalent single degree of freedom damped mass spring system when subjected to a dynamic harmonic force $P(t)=P_0\sin(\omega t)$ can be determined using Equation 4.

$$M_e z''(t) + C_e z'(t) + K_e z(t) = P(t) \tag{4}$$

where $z(t)$, $z'(t)$ and $z''(t)$ are the relative displacement, relative velocity and acceleration of equivalent SDOF system at time t, respectively.

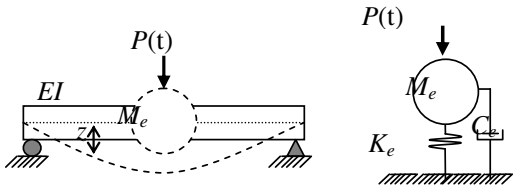

Figure 1. Simply supported RC beam and its equivalent SDOF model .

The dynamic response of the SDOF system to the harmonic load $P(t)$ includes complimentary and particular parts. The complimentary response is transient vibration and can be ignored if the dynamic force be exerted long enough. The particular response is considered as steady state vibration and subject to the initial condition can be written as Equation 5 [20-22]:

$$z(t) = \frac{p_o}{K_e}.\frac{1}{\sqrt{(1-\beta^2)^2 + (2\xi\beta)^2}}.\sin(\omega t - \alpha) \tag{5}$$

where $P_0 = me\omega^2$, $\beta = \omega/\omega_n$, $\alpha = \tan^{-1}[\xi\beta / (1-\beta^2)]$ and m is the eccentric mass attached to the two flywheels of vibrating motor at eccentricity e rotating with angular velocity ω, natural angular frequency $\omega_n = (K_e / M_e)^{0.5}$ and ξ is the damping ratio of the equivalent system.The maximum displacement z_{max} occurs when $\sin(\omega t-\alpha) = 1$. Therefore, at resonance ($\beta = 1$), z_{max} may be obtained using Equation 6.

$$z_{\max} = \frac{me\omega^2}{K_e} \cdot \frac{1}{2\xi} = \frac{me\omega_n^2}{K_e} \cdot \frac{1}{2\xi} \tag{6}$$

Equation 6 can be rewritten as Equation 7.

$$\frac{me\omega_n^2}{2\xi} = K_e \cdot z_{\max} \tag{7}$$

The right hand side of Equation 7 can be considered as equivalent static force. Consequently, a load displacement curve can be obtained through resonance testing ($\omega = \omega_n$) by varying the value of the product $m*e$ and measuring the maximum vibration amplitude at the center of the beam where the vibrating motor is situated, and then plotting the equivalent static force against maximum amplitude z_{max}.
Alternatively if a stiffness K_0 corresponding to a frequency $\omega_{0n} = (K_{0e} / M_e)^{0.5}$ is known for the first value of $m \times e$, the load displacement curve may be found using Equation 8.

$$\left(\frac{\omega_n^2}{\omega_{0n}^2}\right) = \frac{K_{0e}}{K_e} \Rightarrow K_{0e}\left(\frac{\omega_n}{\omega_{0n}}\right)^2 z_{\max} = K_e . z_{\max} \tag{8}$$

where, $K_e = K_{0e} (\omega_n / \omega_{0n})^2$.

Equation 8 assumes that the equivalent dynamic mass M_e is constant and independent of amplitude of response.
In this paper two methods are proposed for obtaining load displacement curves through dynamic testing for in situ RC beams using Equations 7 and 8. Dynamic stiffness given by these Equations can be expressed as Equations 9 and 10.

$$K_{1D} = \frac{me\omega_n^2}{2\xi\, z_{\max}} \tag{9}$$

$$K_{2D} = K_{0D}\left(\frac{\omega_n}{\omega_{0n}}\right)^2 \tag{10}$$

These methods may be considered as alternatives to expensive and more time consuming static tests for damage detection of RC beams. The first method is depending on natural frequency, damping and vibration amplitude for the any value of $m \times e$. But, the second method only is depending on natural frequency and independent of damping and amplitude.

So, in this study the damping ratio ξ is obtained experimentally from a decay function using the logarithmic decrement method (LDM) and Equation 11 [20,22]. Logarithm decrement δ is a measure of the rate of decay of Free-vibration response.

$$2\xi = \frac{\delta}{\pi} = \frac{1}{\pi N} Ln\left[\frac{z_q}{z_n}\right] \tag{11}$$

where z_n and z_q are the displacement amplitude of vibration of the beam after n and q cycles respectively, and $N = n - q$.

3 INSTRUMENTATIONS

A 27 kgs vibration motor was used for exerting harmonic dynamic point loads of $P(t) = me\omega^2 \sin \omega t$ at the center of RC beams. The motor was fitted with two circular aluminum flywheels with attachments for eccentric masses m at eccentricity e. The angular velocity of motor ω could be varied through a frequency converter by means of two potentiometers for coarse and fine variations. A displacement transducer was used for measuring the vertical dynamic displacements $z(t)$ at mid span of the beams. A view of the vibration motor is given in Fig. 2.

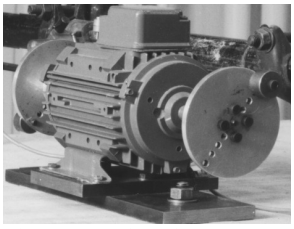

Figure 2. Vibration motor and eccentric mass attached to its flywheels.

A calibrated hydraulic jack with a capacity of 10 tons was used for exerting static point loads at mid span of the test beam. The load was transmitted through a load-cell and thick metal plate on the beam. This kind of loading system is the most common type of loading arrangement and is favored for laboratory experiments because it has the advantage of offering a substantial region of nearly uniform moment coupled with very small shears [23]. All experiments conducted on the beam used the point loading test set-up as seen in Fig. 3.

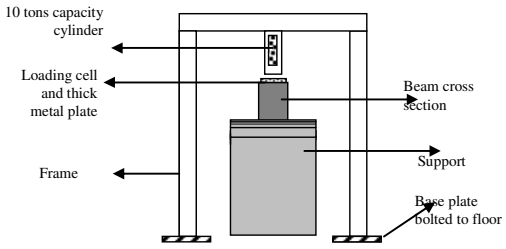

Figure 3. The static point loading test set-up (cross section)

Dial gauges were used for measuring the vertical static displacements. A data logger and a computer were used for actuating and analyzing the data.

4 TEST SPECIMEN AND END SUPPORT DETAILS

One reinforced concrete beam of 4m long, 30cm wide, and 40cm deep was made for tests. The geometry and cross section of the beam are shown in Fig. 4. The reinforcements in the beam consisted of three 16 mm diameter tension reinforcement bars and two 12 mm diameter compression reinforcement bars running the length of the beam. Shear reinforcements consist of vertical stirrups of 8 mm diameter at every 20cm. Total mass of the beam is about 1152 kg which results in a density of $\rho = 2500$ kg/m^3. The material properties are taken form structural concrete. The design compressive strength f'_c = 200 kg/cm², the elastic modules E = 2.1E6 kg/cm², the cracking moment M_{cr} = 2460 kg-m and the related load is equal to 2041 kg. Preventing deflection of the reinforcement, preventing slippage between the reinforcement and adjacent concrete and insuring removal of air are some factors that were considered in making the RC beam. Rectangular cross-section is used to avoid coupling any effect between horizontal and vertical bending modes.

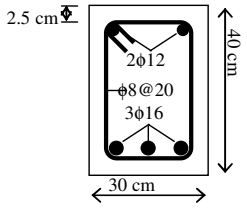

Figure 4. The geometry and cross section of the beam.

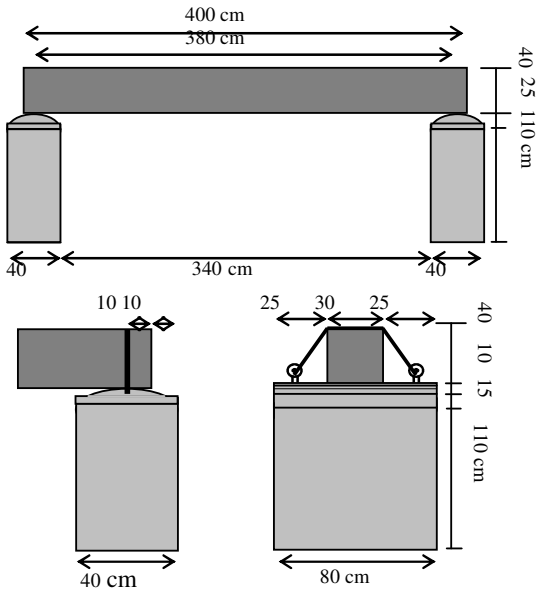

Figure 5. Overall end conditions and support details of beam.

Fig. 5 shows the overall end conditions of the beam. The beam is simply supported on two concrete blocks with horizontal cross section of 40 × 80 cm and height of 110 cm and is cantilevered 10 cm at each end. Two hooks are mounted on the supports, and cable anchorage has been used to prevent beam taking off from the supports during dynamic tests.

5 TEST PROCEDUER

Mid span force-displacement curves were obtained statically and dynamically for increasing degree of cracking. The dynamic force-displacement curves were obtained from steady state vibration at resonance using Equations 7 and 8. The variation in natural angular frequency and amplitude of beam response with increasing pulsating dynamic force were determined by increasing the eccentric mass m from 38.6 to 147.4 grams at eccentricity e = 61 mm. The steady state vibration for each case of eccentric mass was terminated by switching off the vibrator to obtain the decay function from which the damping ratio was calculated by the LDM and the equivalent static force was calculated from $me\omega_n^2/2\xi$. Static Force-displacement curves are obtained by application of an increasing concentrated load at mid span.

The tests procedure included the following 7 steps. The experimental stages are also shown schematically in Fig. 5:

1- Increasing static point load up to Q kg is applied gradually at mid span and corresponding vertical static displacements of mid span are measured using static dial gauges. Static force-displacement curves are plotted for increasing concentrated load at mid span.

2-The static load Q is taken off gradually and static displacements of mid span are measured. Static force-displacement curves are obtained for decreasing (unloading) concentrated load at mid span. Then, steps 3 to 6 are repeated.

3- Using the vibration motor and a specified eccentric mass m and eccentricity e, a dynamic force of $P(t) = me\omega^2 \sin \omega t$ is applied at the mid span of the beam.

4- The angular frequency of the dynamic force is adjusted to the natural angular frequency of the beam so that ($\omega = \omega_n$) and the beam vibrates at resonance. The motor is left on for long enough to obtain the maximum steady state vibration amplitude at resonance. The maximum amplitude of vibration z_{max} and ω_n (or f_n) are recorded using the dynamic displacement transducer.

5- The vibration motor is turned off so that the beam starts free damped vibration and the history of changes of amplitude of vibration $z(t)$ by time t is recorded. From this decay function, damping ratio is calculated using LDM.

6- For six different eccentric mass values m = 38.6, 64.5, 86.2, 102.0, 120.2 and 174.4 grams and constant eccentricity e = 61 mm steps 3 to 5 are repeated. Dynamic Force-displacement curves are obtained using Equation 9 by plotting $me\omega_n^2/2\xi$ against the maximum amplitude of vibration z_{max} and using Equation 10 by plotting, $K_{0D}\,(\omega_n/\omega_{0n})^2\,z_{max}$ against z_{max}.

7- For five different static point loads Q = 0.0, 2.0, 2.5, 3.12, and 3.7 tons steps 1 to 5 are repeated. The beam is statically loaded by one point load with a hydraulic jack at the center of beam. An increasing static loading is applied to produce successive damage. The displacement in the center of beam is recorded by an LVDT installed under the beam as shown in Fig. 6. After each static load step, the beam sides and under surface were visually inspected to locate and quantify the cracks. The experiment results for Q = 0.0 is taken as reference for uncracked beam condition. The other values of Q greater than 0.0 represent conditions that cracks are developed and progressed successively.

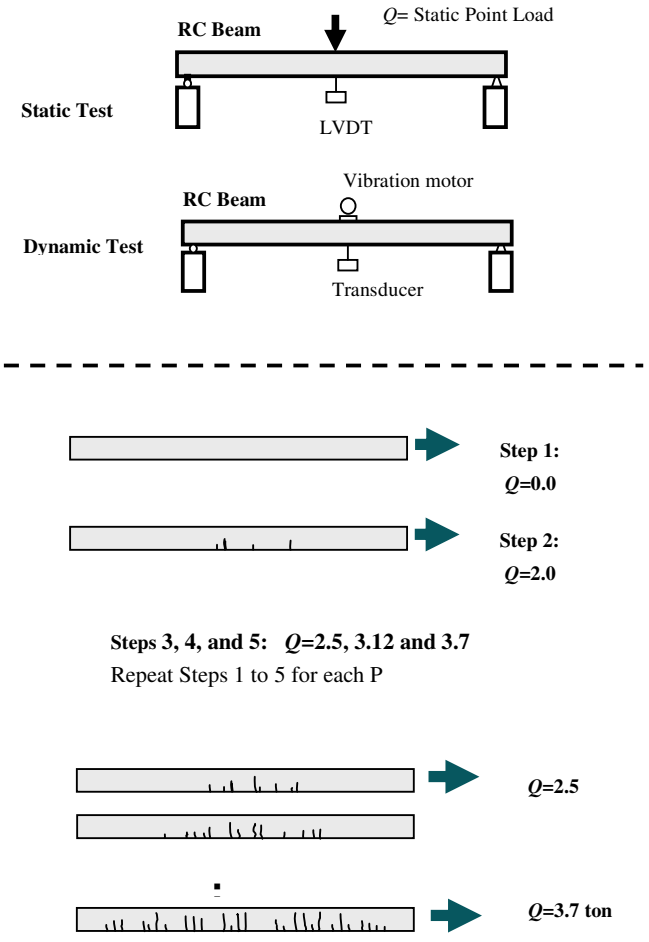

Figure 6. Schematic diagram of experimental static and dynamic tests procedure.

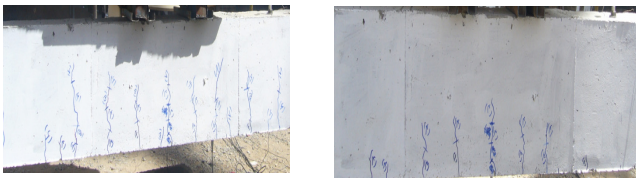

Figure 7. Crack pattern photographs

For each static load step, the bending stiffness of the beam is obtained by Force-deformation curve and also the crack pattern is studied by visual inspection. As a sample, crack pattern photograph was taken of the beam for the step 4 as shown in Fig. 7.

6 EXPERIMENTAL TEST RESULTS AND DISCUSSIONS

6.1 Dynamic and static stiffness

Static Force-displacement curves are plotted for increasing concentrated load at mid span as shown in Fig. 8. The secant flexural stiffness of beam decreases with increasing static point load and therefore with increasing degree of cracking.

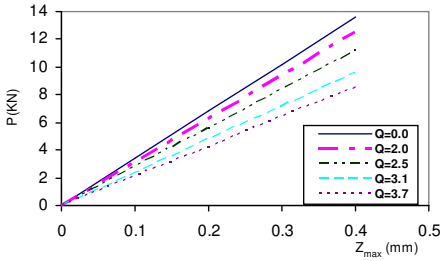

Figure 8. The static force-displacement curves for any step of loading.

For five different static point loads Q = 0.0, 2.0, 2.5, 3.12, and 3.7 tons, steps 1 to 5 of test procedure are repeated and dynamic characteristics of the beam including f_n, z_{max} and ξ are calculated. Damping ration ξ is calculated using LDM as stated in Equation 9 for different values of N=5, 10, 15, 20, 30 35, and 40 cycles. Then the average values are also calculated and the results are tabulated. As an example, Table 1 shows the dynamic characteristics of the RC beam for uncracked condition when the static point load Q =0.0 ton. The results indicate that the natural frequency of beam decreases, its maximum amplitude of vibration increases and damping ratio increases with increasing eccentric mass and therefore with increasing dynamic load. The test results confirm the fact that the maximum amplitude of vibration increases with increasing dynamic load. Also, show decreasing natural frequency and increasing damping ratio with increasing dynamic load that can help in dynamic assessment of RC beams. Variations of damping ratio 2ξ against the number of cycles N used in LDM for different static point loads Q = 0.0, 2.0, 2.5, 3.12, and 3.7 tons are shown in Fig. 9a.

Table 1. Dynamic characteristics for the uncracked beam, Q=0.0 and e=61 mm.

$m_{(grams)}$	$f_{(Hz)}$	$z_{(mm)}$	2ξ (%)								
			N=5	10	15	20	25	30	35	40	Ave.
38.6	36.87	0.159	2.992	2.632	2.556	2.496	2.416	2.359	2.260	2.260	**2.496**
64.5	36.76	0.233	4.224	3.619	3.304	3.135	3.011	2.827	2.696	2.632	**3.181**
86.2	34.44	0.257	4.224	3.775	3.804	3.498	3.396	3.065	2.833	2.706	**3.413**
102	36.02	0.316	4.813	4.023	3.848	3.699	3.476	3.326	3.177	3.046	**3.676**
120.2	35.71	0.342	4.873	4.456	4.253	3.947	3.785	3.326	2.992	2.992	**3.828**
174.4	35.41	0.389	5.949	4.552	4.412	4.202	3.909	3.648	3.355	3.202	**4.154**
Ave.			**4.513**	**3.843**	**3.696**	**3.496**	**3.332**	**3.092**	**2.886**	**2.806**	

Also, variations of damping ratio 2ξ against the number of cycles N for increasing eccentric masses are plotted and Figs. 9a, 9b and 9c are presented here as examples. It is found that the damping ratio ξ is significantly influenced by the degree of cracking, increase of eccentric mass m and number of cycles N. Therefore, the damping value obtained by this approach is an approximate value and is based on many assumptions.

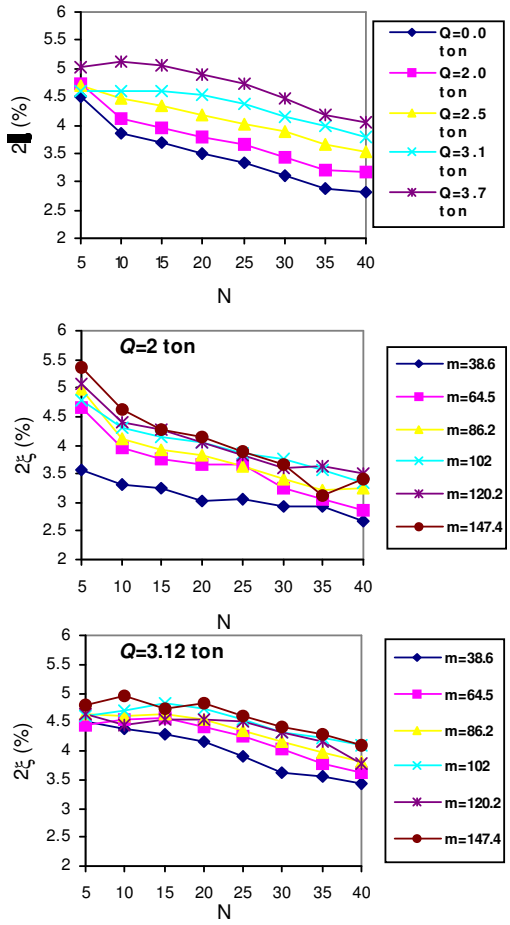

Figure 9. Variations of damping ratio with increasing number of cycles N for different Q and m.

This type of damping is often as referred as effective damping [22]. It is possible to calculate the average of damping ratio for both different masses and different cycles. The last row of Table 1 and graphs of Fig. 9a indicate that damping ratio decreases with increasing number of cycles N.

For five different static point loads Q = 0.0, 2.0, 2.5, 3.12 and 3.7 tons steps 1 to 6 of test procedure are repeated and dynamic Force-displacement curves are obtained using six different values of eccentric mass m and first proposed method i.e. Equation 9 by plotting $me\omega_n^2/2\xi$ against the maximum amplitude of vibration $z_{\max}$ and the results are tabulated. Table 2 shows the results for the condition where there is no static point load i.e. Q = 0.0 as an example. Dynamic Force-displacement curves are also obtained using second proposed method i.e. Equation. 10 and plotting $K_{0D}\ (\omega_n / \omega_{0n})^2\ z_{\max}$ against $z_{\max}$. Table 3 shows the results for the condition where there is no static point load i.e. Q = 0.0 as an example.

Fig. 10 shows the secant stiffness curves obtained by these two proposed methods for all values of Q indicating the un-cracked and cracked conditions. The effect of considering different number of cycles N to obtain damping ratio is shown on each graph and dynamic secant stiffness curves are compared with the static force displacement curves.

Results indicate that by increasing the number of cycles N to LDM, the dynamic Force-displacement curve closes to the static Force-displacement curve. For graphs obtained using the second proposed method the static stiffness value is mainly near to dynamic stiffness values acquired for 35 and 40 cycles. Whereas, the static stiffness value in the graphs calculated using the first proposed method is mainly more than the dynamic stiffness value obtained for 40 cycles. Consequently, for using the first proposed method, the stiffness value resulted from 40 cycles and for using the second proposed method, the average of stiffness value obtained from 35 and 40 cycles have been selected as dynamic stiffness.

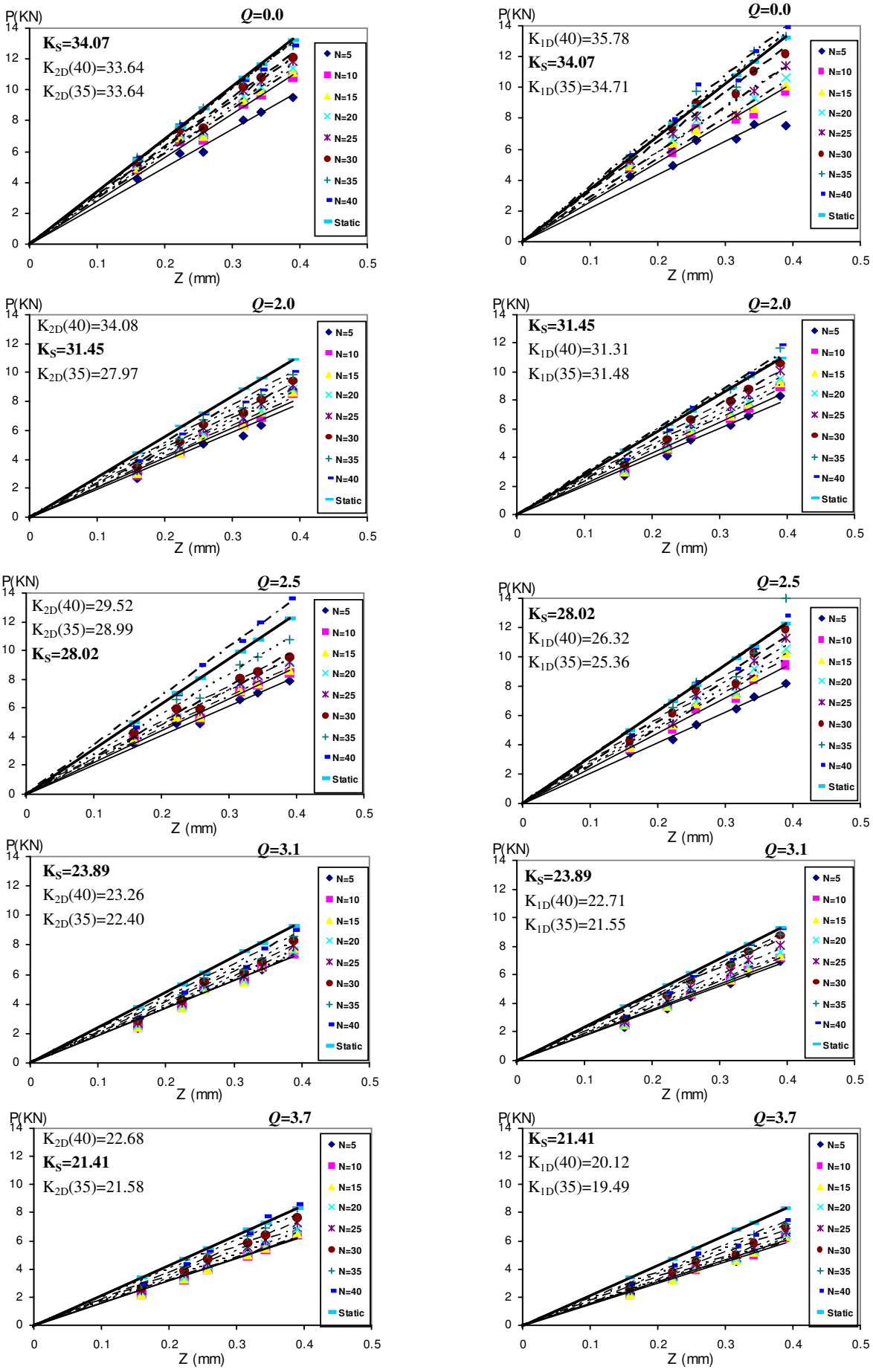

Figure 10. Secant stiffness curves obtained by the two proposed methods for uncracked and cracked beam.

Table 2. Experimental test results using Equation 9 for condition Q=0.0 and e=61 mm.

m(grams)	f(Hz)	z(mm)	2ξ (%)								
			N=5	10	15	20	25	30	35	40	Ave.
38.6	36.87	0.159	4.224	4.802	4.944	5.063	5.231	5.357	5.592	5.592	**5.101**
64.5	36.76	0.233	4.919	5.799	6.352	6.695	6.970	7.424	7.785	7.974	**6.746**
86.2	34.44	0.257	6.527	7.303	7.247	7.881	8.118	8.995	9.731	10.19	**8.249**
102	36.02	0.316	9.622	7.922	8.282	9.616	8.169	9.582	10.03	10.46	**8.836**
120.2	35.71	0.342	7.575	8.284	8.680	9.353	9.753	11.10	12.34	12.33	**9.928**
174.4	35.41	0.389	7.482	9.778	10.09	10.59	11.39	12.20	13.27	13.90	**11.09**
Ave.			**6.233**	**7.315**	**7.599**	**8.033**	**8.438**	**9.110**	**9.791**	**10.08**	

Table 3: Experimental test results using Equation 10 for condition Q=0.0 and e=61 mm.

m(grams)	f(Hz)	z(mm)	2ξ (%)								
			N=5.	10	15	20	25	30	35	40	Ave.
38.6	36.87	0.159	4.224	4.802	4.944	5.063	5.231	5.357	5.592	5.592	**5.101**
64.5	36.76	0.233	5.888	6.694	6.892	7.057	7.292	7.467	7.795	7.795	**7.110**
86.2	34.44	0.257	5.957	6.772	6.973	7.141	7.377	7.555	8.829	8.829	**7.429**
102	36.02	0.316	8.011	9.107	9.371	9.602	9.921	10.16	10.61	10.61	**9.673**
120.2	35.71	0.342	8.521	9.688	9.974	10.214	10.55	10.81	11.28	11.28	**10.29**
174.4	35.41	0.389	9.530	10.835	11.155	11.423	11.80	12.09	12.91	12.91	**11.58**
Ave.			**7.022**	**7.983**	**8.219**	**8.417**	**8.696**	**8.916**	**9.502**	**9.502**	

Table 4: Static and dynamic stiffness calculated from both proposed methods for different Q.

Load step	Static load Q (ton)	Static Stiffness (KN/mm)	Dynamic Stiffness (KN/mm)	
		k_s	k_{1D} for ξ^{40}	k_{2D} for Ave. (ξ^{35}, ξ^{40})
1	0.0	34.07	35.78	36.64
2	2.0	31.45	31.31	31.03
3	2.5	28.02	26.32	29.26
4	3.12	23.89	22.71	22.83
5	3.7	21.41	20.12	22.13

Theses results have been summarized in Table 4. Fig. 11 shows points obtained for dynamic stiffness from both methods and static stiffness. The best line has been fitted to them. Accordingly, precision and accuracy of the both proposed methods are verified. It is observable that the results related to the second proposed method for dynamic stiffness have best correlation with the static stiffness results.

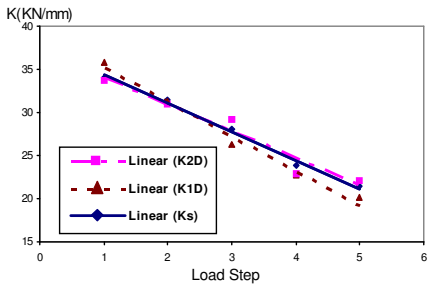

Figure 11. Change of stiffness resulted from dynamic and static testing against load step

6.3 Dynamic Characteristic

The dynamic characteristics of the beam including natural frequency, maximum amplitude of vibration and damping ratio for all five values of Q and six values of m are summarized in Table 5. Damping ratio values in this table are obtained using average value of 35 and 40 cycles. Variations of these characteristics against m (increasing of dynamic force) are plotted in the graphs of Fig. 12. Graphs 12a, 12b and 12c indicate that in every step of loading, by increasing the dynamic force (m), the natural frequency decreases, and the vibration amplitude and the damping ratio increases, respectively.

Table 6 and Fig. 13 show the variation of total averaged dynamic characteristics of the beam for all five static load steps i.e. Q =0.0, 2.0, 2.5, 3.12 and 3.7 ton. The results indicate that vibration amplitude, bending stiffness and natural frequency of the beam decreases and damping ratio increases with increasing degree of cracking. It can be observed that the rate of decaying amplitude of vibration is linear, indicating that damping from micro cracking is more important than viscous damping [6,22] .

Load Step	1 (Q=0.0)			2 (Q=2.0)			3 (Q=2.5)			4 (Q=3.12)			5 (Q=3.7)		
m	f	z_{max}	2ξ	f	z_{max}	2ξ	f	z_{max}	2ξ	f	z_{max}	2ξ	f	z_{max}	2ξ
(grams)	*(Hz)*	*(mm)*	*(%)*	*(Hz)*	*(mm)*	*(%)*	*(Hz)*	*(mm)*	*(%)*	*(Hz)*	*(mm)*	*(%)*	*(Hz)*	*(mm)*	*(%)*
38.6	36.8	0.16	2.26	36.6	0.13	2.69	35.2	0.12	3.00	34.2	0.11	3.55	33.0	0.11	3.47
64.5	36.7	0.22	2.63	35.9	0.20	2.86	34.5	0.20	3.26	33.3	0.19	3.61	32.0	0.18	3.76
86.2	34.4	0.26	2.71	35.5	0.26	3.17	34.2	0.25	3.44	33.0	0.24	3.74	31.5	0.22	4.05
102	36.0	0.32	3.00	35.3	0.31	3.34	33.9	0.30	3.57	32.7	0.29	4.00	31.2	0.29	4.23
120.2	35.7	0.34	3.00	35.1	0.35	3.34	33.6	0.34	3.72	32.3	0.34	4.00	30.8	0.32	4.29
147.4	35.4	0.39	3.20	34.8	0.41	3.36	33.2	0.41	3.88	32.0	0.40	4.05	30.5	0.39	4.41
Total Ave.			**2.8**			**3.12**			**3.48**			**3.83**			**4.04**

Table 5. Dynamic characteristics of the beam for all five load steps Q.

6.4 Test results verification

The structure under consideration is a simple supported beam of length L = 380 cm, density ρ = 2500 kg/m^3, cross section A = 1200 cm^2 and bending stiffness EI = 3.36E11 kg-cm. Hence, the theoretical undamped natural frequency for the first mode at load step 1 equals [21].

$$f_1 = \frac{\pi}{2L^2}\sqrt{\frac{EI}{\rho A}} = 36.4\ (Hz) \qquad (12)$$

As regards ξ = 0.014 is small, the theoretical damped natural frequency gives f = 36.8 Hz against 36.8 Hz outcome test. Therefore, the accuracy of experimental results is approved.

7 CONCLUSION

The results indicate that secant flexural stiffness of beam decreases with increasing static point load and therefore with increasing degree of cracking. The natural frequency of beam mostly decrease and its maximum amplitude of vibration increase with increasing eccentric mass and therefore with increasing dynamic load. The damping ratio ξ is significantly influenced by the degree of cracking, increase of eccentric mass m and number of cycles N. In general, damping ratio ξ calculated by averaging the values for different cycles, increases with increasing degree of cracking and with increasing dynamic load. It was observed that rate of decaying amplitude of vibration is linear, indicating that damping from micro cracking is more important that viscous damping The results indicate that maximum amplitude of vibration, bending stiffness and natural frequency of beam decrease and damping ratio increases with increasing degree of cracking.

For five different static point loads Q = 0.0, 2.0, 2.5, 3.12 and 3.7 tons steps 1 to 6 of test procedure are repeated and dynamic secant flexural Force-displacement curves are obtained using six different values of eccentric mass m and first proposed method i.e. Equation 9 and also by using second proposed method i.e. Equation 10. Precision and accuracy of the both proposed methods are verified. It is observable that the results related to the 2nd proposed method for dynamic secant stiffness curves have best correlation with the static stiffness curves. Results indicate that by increasing the number of cycles N in logarithmic decrement method, the dynamic Force-displacement curve closes to the static Force-displacement curve. The proposed methods are

limited to conditions where forced excitations are allowed.

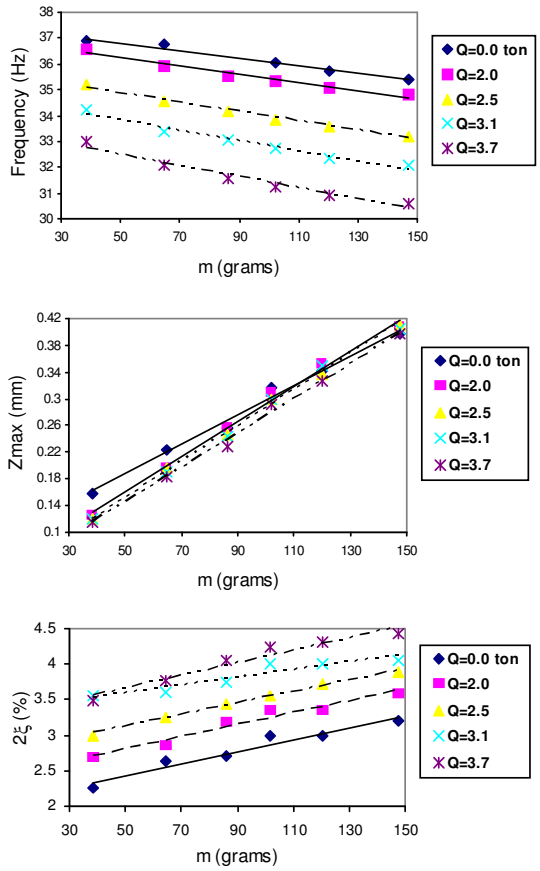

Figure 12. Variation of natural frequency, maximum amplitude of variation and damping ratio with eccentric mass *m*

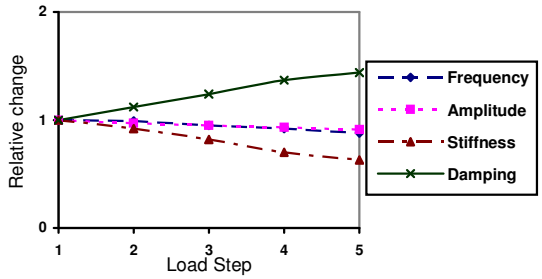

Figure 13. Variations of the relative decrease of dynamic characteristics with increasing degree of cracking

8 REFERENCES

1. Doebling, S., Farrar, C., and Prime, M., "A Summery review of vibration-based damage identification methods", *Shock Vib. Dig.,* **30**(2), 1998, pp. 91–105.
2. Turner, J.D. and A.J. Pretlove, "A Study of the Spectrum of Traffic-Induced Bridge Vibration", *Journal of Sound and Vibration,* **122,** 1988, pp. 31–42.
3. Spyrakos, C., H.L. Chen, J. Stephens, and V. Govidaraj, "Evaluating Structural Deterioration Using Dynamic Response Characterization", *Proc. Intelligent Structures, Elsevier Applied Science*, 1990, pp. 137–154.
4. Ren, W. X., and De Roeck, G., "Structural damage identification using modal data. I: Simulation Verification", *J. Struct. Eng.,* **128**(1), 2002, pp. 87-95.
5. Ren, W. X., and De Roeck, G., "Structural damage identification using modal data. II: Test Verification", *J. Struct. Eng.,* **128**(1), 2002, pp. 96-104.
6. Daneshjoo, F., and Karimi, Y., "Investigation of Influence of Increasing Crack in dynamic behavior of Concrete Beams", *3rd International Conference on Concrete, Amirkabir University*, Tehran, Iran, 2000.
7. Ndambi Mulambula J.-M., "Damage assessment in reinforced concrete beams by damping analysis", *Ph.D. thesis*, Vrije University, Brussel, Belgium, 2002.
8. Salane H.J., Baldwin J.W., "Identification of modal properties of bridges", *Journal of Structural Engineering,* **116**(7), 1990, pp. 2008-2021.
9. Casas J.R., Aparicio A.C., "Structural damage identification from dynamic - test data", *Journal of Structural Engineering,* **120**(8), 1994, pp. 2437-2450.
10. Williams C., Salawu O.S., "Damping as a damage indication parameter", *Proceedings of 15th International Modal Analysis Conference, Orlando, FL, USA,* 1997, pp. 1531-1536.
11. Kato, M. and S. Shimada, "Vibration of PC Bridge during Failure Process", *ASCE Journal of Structural Engineering,* **112**, 1986, pp. 1692–1703.
12. Aktan, A.E., K.L. Lee, C. Chuntavan and T. Aksel, "Modal Testing for Structural Identification and Condition Assessment of Constructed Facilities", *Proc. of 12th International Modal Analysis Conference,* 1994, pp. 462–468.
13. Farrar, C.R., W.E. Baker, T.M. Bell, K.M. Cone, T.W. Darling, T.A. Duffey, A. Eklund, and A. Migliori, "Dynamic Characterization and Damage Detection in the I-40 Bridge over the Rio Grande", Los Alamos National Laboratory report LA, 12767-MS, 1994.
14. Peeters B., "System Identification and Damage Detection Civil Engineering", *Ph.d. thesis*, K.U.Leuven, Belgium, 2000.
15. Teughels A., "Inverse Modelling of Civil Engineering Structures Based on Operational Modal Data", *Ph.d. thesis*, K.U.Leuven, Belgium, 2003.
16. Maeck J., "Damage Assessment of Civil Engineering Structures by Vibration Monitoring", *Ph.d. thesis*, K.U.Leuven, Belgium, 2003.
17. Mirdamadi, H., and Alibeigi, M., "Model Updating of Dynamic F.E. model in Bridge Structures", *M.S. thesis*, Esfahan Univ. of Technology, Esfahan, Iran, 2003.
18. Bakhtiar-Nejad, F., Rahai, A., Esfandiari, A., "Theoretical and Experimental Damage Detection Method of Structures Using Static Displacements", *International Journal of Civil Engineering,* **2**(2), 2004, pp. 112-122.
19. Bolton, R., Sikorsky, C., Park, S., Choi, S., and Stubbs, N., "Modal Property Changes of a Seismically Damaged Concrete Bridge", *J. Bridge Engineering,* 2005, pp. 415-428.
20. Chopra, A. K., 2001, *Dynamics of Structures Theory and Applications to Earthquake Engineering*, Prentice Hall International Inc..
21. Roy, R. and Craig, Jr., 1981, *Structural Dynamics: an Introduction to computer methods, Research*, New York, John Wiley & Sons, Inc..
22. Wilson, E. L., (3rd ed.), 2002, *Three-Dimensional Static and Dynamic Analysis of Structures*, Berkeley, California, Computers and Structures, Inc..
23. Bungey, J. H., Millard, S.G., 1996, *Testing of concrete in structures,* Cambridge, Blackie academic & professional